Assimilating AMSU-A Radiances in the TC Core Area with NOAA Operational HWRF (2011) and a Hybrid Data Assimilation System: Danielle (2010)

MAN ZHANG, MILIJA ZUPANSKI, AND MIN-JEONG KIM

Cooperative Institute for Research in the Atmosphere, Colorado State University, Fort Collins, Colorado

JOHN A. KNAFF

NOAA/Center for Satellite Applications and Research, Fort Collins, Colorado

(Manuscript received 29 November 2012, in final form 30 April 2013)

ABSTRACT

A regional hybrid variational–ensemble data assimilation system (HVEDAS), the maximum likelihood ensemble filter (MLEF), is applied to the 2011 version of the NOAA operational Hurricane Weather Research and Forecasting (HWRF) model to evaluate the impact of direct assimilation of cloud-affected Advanced Microwave Sounding Unit-A (AMSU-A) radiances in tropical cyclone (TC) core areas. The forward components of both the gridpoint statistical interpolation (GSI) analysis system and the Community Radiative Transfer Model (CRTM) are utilized to process and simulate satellite radiances. The central strategies to allow the use of cloud-affected radiances are (i) to augment the control variables to include clouds and (ii) to add the model cloud representations in the observation forward models to simulate the microwave radiances. The cloudy AMSU-A radiance assimilation in Hurricane Danielle's (2010) core area has produced encouraging results with respect to the operational cloud-cleared radiance preprocessing procedures used in this study. Through the use of the HVEDAS, ensemble covariance statistics for a pseudo-AMSU-A observation in Danielle's core area show physically meaningful error covariances and statistical couplings with hydrometeor variables (i.e., the total-column condensate in Ferrier microphysics). The cloudy radiance assimilation in the TC core region (i.e., ASR experiment) consistently reduced the root-mean-square errors of the background departures, and also generally improved the forecasts of Danielle's intensity as well as the quantitative cloud analysis and prediction. It is also indicated that an entropy-based information content quantification process provides a useful metric for evaluating the utility of satellite observations in hybrid data assimilation.

1. Introduction

Tropical cyclone (TC) is a generally inclusive term that includes hurricanes in the Atlantic basin and typhoons in the western Pacific. As one of the most destructive natural hazards on Earth, TCs are often accompanied by severe winds, torrential rainfall, and flooding and can dramatically impact a society.

Given their enormous economic and social impacts, the demand for more accurate TC track and intensity forecasts with longer lead times is greater than ever. Over the past two decades, significant progress has been made in TC track prediction but TC intensity and structure forecasts remain a challenge for most operational numerical weather prediction (NWP) centers (DeMaria 2009). The apparent lag in skills between track and intensity forecasts is the result of many factors. First of all, vortex initialization in the current generation of hurricane models [e.g., Hurricane Weather Research and Forecasting (HWRF), Geophysical Fluid Dynamics Laboratory (GFDL)], which appears to work well for synoptic-scale TC forecasts, is not adequate for creating realistic vortex structures. One of the reasons is that these same models do not assimilate high-resolution observations in the core region of TCs, which can be a key to intensity prediction (e.g., Rogers et al. 2006; Zhang et al. 2009). Observational analyses (Wakimoto and Black 1994; Gall et al. 1998) and numerical simulations (Yau et al. 2004; Rogers 2010) indicate that hurricanes often

Corresponding author address: Dr. Man Zhang, NOAA/Earth System Research Laboratory, Global Systems Division, 325 Broadway, Boulder, CO 80303.
E-mail: man.zhang@noaa.gov

DOI: 10.1175/MWR-D-12-00340.1

have strong asymmetries in deep convection in the eyewall and in the spiral rainbands. In general, these clouds in a TC are intricately connected with the dynamics of the cyclone itself. As indicated in an idealized but typical array of rainbands and eyewall in a TC in Houze (2010, Fig. 30), the inner-core region with an approximately 150-km radius is dynamically constrained by the strong cyclonic vortex circulation, while the outer-core region is the ambient region of the vortex, depicted as broken lines of convective cells spiraling around the TC. Kurihara et al. (1993) found that adding the asymmetric component to the axisymmetric vortex yields marked improvements in the forecasting of hurricane track and intensity. One potential solution to this problem is in assimilating remotely sensed observations of clouds into the TC core area, especially when the storm is over the open ocean where there are not sufficient in situ observations available.

Recently, considerable effort and progress has been made in the area. Through the Advanced Research core of the Weather Research and Forecasting Model (ARW-WRF; Skamarock et al. 2005) with its three-dimensional variational data assimilation system (3DVAR; Barker et al. 2004), Xiao et al. (2009) and Pu et al. (2009) successfully assimilated airborne Doppler radar (ADR) data into the TC core area. Both studies highlighted a need for data assimilation techniques with vortex-specific flow-dependent forecast error estimations, such as the ensemble Kalman filter (EnKF) or 4DVAR. More recently, using a WRF-based EnKF data assimilation system, Zhang et al. (2011) examined the assimilation of high-resolution ADR observations for convection-permitting hurricane initialization and forecasting in real time and showed a very promising level of performance over the past three Atlantic hurricane seasons in terms of averaged mean absolute intensity forecast errors. However, ADR observations are only occasionally available when National Oceanic and Atmospheric Administration (NOAA) research aircraft are conducting hurricane reconnaissance.

As an essential part of the earth observing system, satellite observations are ideal for TC studies because of the temporal and spatial coverage. Currently, the cloud-cleared radiance assimilation has become a routine practice in most NWP centers. Cloud-cleared radiance observations are important since they provide critical information about the temperature and water vapor structure surrounding cloudy and rainy areas. However, using only cloud-cleared data represents a major underutilization of high-cost satellite instruments, since satellite measurements in cloudy and rainy regions contain valuable information pertinent to the atmospheric hydrological cycle. For TC modeling, cloud-cleared radiance assimilation also does not provide information needed to improve the TC vortex initialization. Such shortcomings have recently led to a growing interest in assimilating satellite observations in cloudy and rainy regions at operational NWP centers (e.g., McNally 2009; Bauer et al. 2010).

In this study, the prototype regional hybrid data assimilation system is based on the 2011 version of the NOAA operational HWRF model (Gopalakrishnan et al. 2011), and the maximum likelihood ensemble filter (MLEF; Zupanski 2005; Zupanski et al. 2008). Specifically, observations from the Advanced Microwave Sounding Unit-A (AMSU-A) (Robel 2009) on board the *NOAA-18* satellite and the European Organization for the Exploitation of Meteorological Satellites (EUMETSAT) *Meteorological Operational-A* (*MetOp-A*) satellite have been utilized. For the purpose of discussion, direct assimilation of cloudy AMSU-A radiances in the HWRF (2011) inner domain with a $6° \times 6°$ domain, which is referred to as the ''TC core area'' in this study. Thus, the TC core area typically covers both the TC's eyewall (i.e., the inner-core region) and its spiral rainbands (i.e., the outer-core region). The current study thus focuses on evaluating the added value of directly assimilating cloud-affected AMSU-A radiances in the TC core area using an operational hurricane guidance model with the goal of developing a coherent framework to assess the optimal set of channels and forward model biases for model state estimation. More specifically this study will (i) examine the performance of the data preprocessing and direct assimilation of the satellite radiances in the TC core area; (ii) assess the value of cloud-affected satellite radiance using Hurricane Danielle (2010); (iii) explore a multivariate description of the ensemble error covariance in the TC core area, especially involving the model hydrometeor variables; and (iv) evaluate an entropy-based information measure for determining the information content of the observation datasets and assessing the effect of forward model uncertainties.

The paper is organized as follows: Section 2 describes the components of the regional hybrid variational–ensemble data assimilation system (HVEDAS) used to assimilate satellite radiances in the TC core area. Section 3 discusses the National Centers for Environmental Prediction (NCEP) operational practice of assimilating cloud-cleared AMSU-A radiances and recent implementations that allow direct assimilation of cloudy AMSU-A radiances. The experiment design is detailed in section 4, and the results of the experiments performed to indicate the performance of the new approach are presented in section 5. The final section provides a summary of the important findings and some concluding remarks.

2. A regional HVEDAS for the TC core: MLEF-HWRF (2011)

Before describing key strategies relevant to direct satellite radiance assimilation in the TC core area, we will first summarize the main components of the system. There are three major components of a typical data assimilation system: the NWP model, the observation (forward) operators, and the data assimilation (DA) algorithm.

a. NWP model: NOAA operational HWRF (2011) model

We employ the atmospheric portion of the NOAA operational HWRF (2011), which is based on the Nonhydrostatic Mesoscale Model (NMM) dynamic solver (Janjić et al. 2001; Janjić 2003). The HWRF (2011) is configured with a parent domain with 27-km horizontal grid spacing and a two-way interactive moving nest with 9-km spacing, covering a total area of 75° × 75° and 6° × 6°, respectively. There are 42 vertical levels with the model top at 50 hPa. Representations of atmospheric physical processes in HWRF (2011) include the modified Ferrier microphysics scheme for the tropics (Ferrier 2005), the simplified Arakawa–Schubert (SAS) cumulus parameterization, surface fluxes over water and land, and atmospheric radiation parameterization (Gopalakrishnan et al. 2011). In particular, the Ferrier scheme predicts changes in water vapor and total condensate in the form of cloud water, rain, cloud ice, and precipitation ice (snow/graupel/sleet).

It is worth mentioning that in 2012 the operational HWRF model has been upgraded to an ocean-coupled triple-nested system operating at 3-km horizontal resolution near the hurricane core, and has improved nesting, dynamics, and physics compared to its earlier versions.[1] Significant improvements in the hurricane track and intensity forecasts have been shown in the Environmental Modeling Center (EMC) retrospective tests for two seasons (2010 and 2011) in both the Atlantic and eastern Pacific basins (Tallapragada et al. 2012; Bernardet et al. 2012).

b. Observation (forward) operators

Since satellite radiances are not components of atmospheric state vectors predicted by NWP models, direct assimilation of radiance data requires a relationship between the model-state vectors and the observed radiances, as well as horizontal interpolation from the model grid to the observations. At present, NCEP operations use a three-dimensional variational data assimilation system named the gridpoint statistical interpolation (GSI; Wu et al. 2002; Kleist et al. 2009) to assimilate satellite radiances, though only in cloud-cleared situations. In this study, however, only the forward component of the GSI system, including data ingestion, thinning, a prescribed bias correction scheme, and quality control procedures was used to process the satellite observations. In other words, the GSI background error covariance, the adjoint model, and minimization were not used in our method.

Satellite observations are simulated in GSI using the Community Radiative Transfer Model (CRTM; Weng 2007). The CRTM, which includes both forward and Jacobian radiative transfer (RT) models for all weather conditions, is widely used in satellite data assimilation and remote sensing applications. Given an atmospheric profile of temperature, variable gas concentrations, and cloud and surface properties, the forward component of the radiative transfer model generates a pseudo-observation of brightness temperature at the observation location. The clear and cloudy cases are treated with different methods in CRTM. In clear-sky mode, a radiative transfer model uses temperature, humidity, and ozone as key inputs. In the presence of clouds, CRTM also has a facility to compute cloud-affected radiances using additional inputs of cloud content profiles, and also to account for emission effects due to hydrometeors (Weng and Liu 2003). The current valid hydrometeor types include water, ice, rain, snow, graupel, and hail. As for GSI, we only utilize the forward component of the CRTM.

c. Hybrid DA algorithm: MLEF

In this study, the maximum likelihood ensemble filter (Zupanski 2005; Zupanski et al. 2008) developed at Colorado State University is used as the data assimilation algorithm. The MLEF is a hybrid variational–ensemble data assimilation system, which combines the advantages of the variational and ensemble-based data assimilation methods. Compared to variational approaches, the HVEDAS uses an ensemble of prior forecasts to estimate the flow-dependent error covariance. Compared to EnKF methods, the HVEDAS addresses the nonlinearity of observation operators by employing an iterative minimization of a cost function. An important advantage of the iterative solution method is in its applications with nonlinear observation operators such as cloud- and precipitation-affected satellite observations.

[1] Readers can refer to EMC HWRF website (available online at http://www.emc.ncep.noaa.gov/index.php?branch=HWRF) for the focal aspects of the HWRF (2012) implementation.

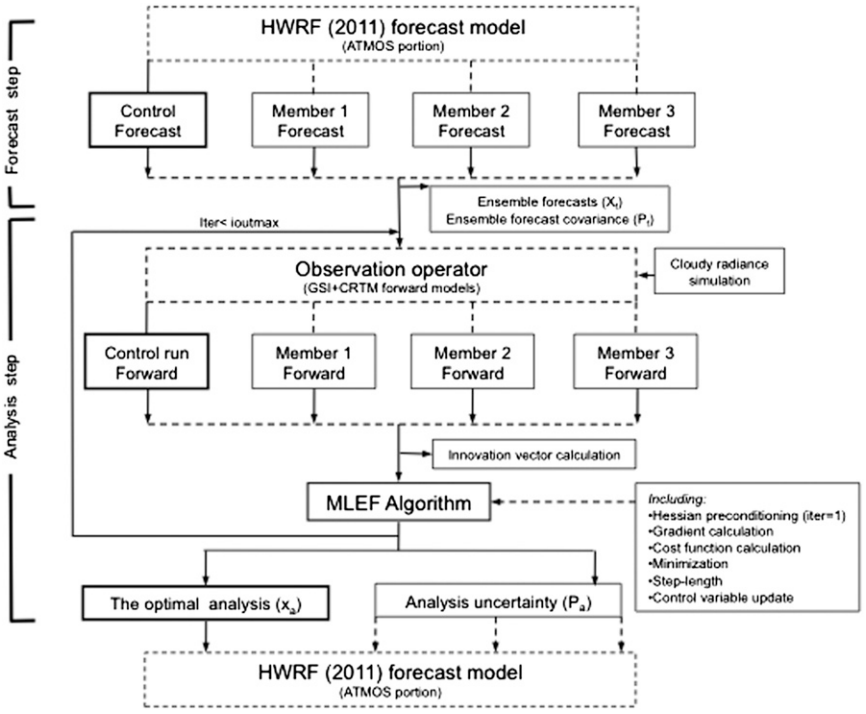

FIG. 1. Schematic diagram of the MLEF-HWRF cycle for a hypothetical three-member ensemble. Each member and control run assimilates the same observational datasets in both the HWRF (2011) inner and outer domains.

The interested reader is directed to Zupanski (2005) for details of MLEF equations.

The current MLEF-HWRF (2011) system was designed to assimilate cloud- and precipitation-affected observations in the TC core area. The forward component of the GSI is adapted to access observations in an NCEP operational environment. One advantage of using the NCEP system to access observations is that we can assimilate all operationally available data. There are two steps in the MLEF-HWRF system (Fig. 1): the forecast and the analysis. In the forecast step, MLEF calls subroutines to run HWRF (2011) ensemble 6-h forecasts to the next analysis time, which are then translated into MLEF state vectors. In addition to the ensemble, an unperturbed forecast initiated from the optimal analysis of the previous cycle is produced as the control forecast. The ensemble perturbation is calculated at the end of the 6-h forecast time from the difference between each ensemble member and the control forecast. In the analysis step, we run an observation-forward model for all ensemble members and the control forecast, and update the forecast perturbations using the MLEF algorithm. At the end of the analysis, MLEF provides both the optimal analysis and uncertainty for this cycle. The updated ensemble perturbations are then added to the control forecast to generate initial ensemble members for the next cycle. The forecast–analysis step is repeated for each of the follow-on cycles.

The initial ensemble at the very beginning of the data assimilation cycles was generated by the time-shifted forecast technique, as described in Zupanski et al. (2008). In the HWRF (2011) application, the parameters at lateral boundaries and the land surface for the outer domains are unperturbed. Examination of the inner domain is of major interest in this study, since it contains the large gradients in pressure, temperature, wind, and moisture that contribute to TC intensity variations and uncertainty.

3. Methodology

In this section, the implementation of cloud-affected AMSU-A radiance assimilation in the TC core area is introduced by explaining how it differs from the current data assimilation practices at NCEP operations [i.e., the Global Forecast System (GFS) model and the operational HWRF system]. The AMSU-A measurements have 15 channels (or frequencies) between 23.8 and 89 GHz. It is generally assumed that microwave sounders (i.e., AMSU-A) are all-weather instruments and are well suited for studying and observing tropical storms (Kidder et al. 2000).

a. AMSU-A radiance assimilation in NCEP operational systems

In this study, AMSU-A 1b radiance data within a 1.5-h time window are ingested into the HWRF (2011) outer and inner domains. The large volume of satellite data and the expense of including them in the analysis usually imply a need for thinning these observations prior to assimilation. The size of the thinning box for the AMSU-A radiances used in this study is 60 km. The individual AMSU-A channels are carefully chosen based on principles of radiative transfer theory. AMSU-A temperature sounding channels in the 50–60-GHz oxygen band (i.e., channels 3–14) respond to the thermal radiation at various altitudes within the atmosphere described by the weighting functions (see Knaff et al. 2000, their Fig. 1). For radiance assimilation in the TC core area, AMSU-A temperature sounding channels are advantageous because they are less sensitive to the presence of clouds when scattering is not detected (i.e., nonscattering clouds), which is a desirable feature for traditional data assimilation methods (i.e., variational methods). However, channels 10–14 are not assimilated in this study because they peak above the top of the HWRF model (i.e., 50 hPa). In turn, AMSU-A channels at 23.8, 31.4, and 89 GHz (i.e., channels 1, 2, and 15), which are located in window regions of the microwave spectrum, are sensitive to the presence of cloud and precipitation, surface emissivity, and water vapor effects. In the GSI forward model, the cloud and precipitation detection procedures use the window channels through a complex multichannel algorithm to indicate the presence of thick clouds or precipitation, and result in the rejection of some or all of the sounding channels at that particular location. Nevertheless, the window channels are of central importance due to their sensitivity to cloud and rain. Additionally, due to the different spatial and temporal coverage patterns of each satellite, *NOAA-18* AMSU-A radiances are captured in the HWRF (2011) inner domain every 12 h with *MetOp-A* radiances occasionally bound in between (Table 2). *NOAA-18* channel 9 and *MetOp-A* channel 7 are used in the quality control process, but not in analysis.

The radiance bias correction procedure may be one of the most important aspects of satellite radiance assimilation. In general, satellite channels may be prone to systematic errors due to instrument or radiative transfer problems, and these biases need to be corrected either before the data enter into the minimization procedure (statistical-based method; Harris and Kelly 2001) or during minimization procedure (variational-based method; Dee and Uppala 2009). Many research papers deal with the removal of these biases and most of them are based on global models and cloud-cleared radiances. Since direct assimilation of satellite radiances with the regional application is still in its infancy, our approach is to take advantage of the radiance bias correction scheme described by Derber and Wu (1998), in which predictor coefficients are already generated for cloud-cleared AMSU-A data using the GFS model. One of the major concerns in using this method for cloudy radiance applications is that it was designed for processing the cloud-cleared radiances, and thus cloudy radiances could be inappropriately corrected.

Although the GSI data assimilation is used for all storms in the NOAA operational HWRF (2012) initialization (Tallapragada et al. 2012; Bernardet et al. 2012), it is employed only for deep storms (classified by TC vitals) in the HWRF (2011) system. However, in both systems, assimilation of conventional data is excluded within a radius of 1200 km around the storm. The utilization of all available datasets, especially storm-scale observations used to define storm intensity and structure, remains a challenge to the operational HWRF modeling system.

b. Toward radiance assimilation in the TC core area

In this study, we have used the GSI data processing procedures for cloud-cleared satellite radiance data assimilation as closely as possible to avoid duplication and maintenance of computer code (e.g., data ingestion and thinning, channel selection, bias correction and quality control). However, some departures are necessary when this scheme is applied to the HWRF (2011) TC core area, where satellite data commonly contain cloudy and/or rainy conditions. In addition to using a hybrid data assimilation method (i.e., MLEF), there are two other strategies required for assimilating cloudy AMSU-A radiances in the TC core area: (i) augmenting control vector to include cloud variables (i.e., the total-column condensate in Ferrier microphysics scheme), and (ii) including cloud-guess profiles in the microwave radiance simulation.

The MLEF control variables are chosen from the HWRF model prognostic variables and include zonal and meridional wind components, temperature, specific humidity, hydrostatic pressure depth, and total-column condensate (CWM). Since CWM is directly related to clouds in HWRF, including this variable allows more realistic adjustment of the analysis to cloudy observations. Also, since very little is known about the forecast error characteristics of the hydrometer variable, implying a difficulty when applying variational methods, it is anticipated that the use of a hybrid methodology will provide an opportunity to explore the error distribution and evolution within the TC vortex scale. On the other hand, if cloud-affected satellite observations are

assimilated, clouds must be derived from the cloudy atmospheric variables by the application of cloud radiative property estimation as part of the forward model. In this study, we take advantage of a prognostic cloud scheme (Hou et al. 2002), which considers liquid and ice phases of the cloud contents, and uses explicitly determined condensate from the first guess to compute cloud radiative properties such as the effective radius of cloud particles. The microphysical properties (i.e., extinction coefficient, single-scattering albedo, and asymmetry factor) of cloud particles are precalculated and stored in lookup tables (Simmer 1994; Macke et al. 1996; Mishchenko et al. 2000; Baum et al. 2005). The Mie theory is assumed in all calculations for spherical liquid and ice water cloud particles, and modified gamma distributions of practical sizes are assumed in the microwave spectral region.

Note that adding model cloud representations may substantially modify the simulated brightness temperatures (TBs), and thus the error characteristics of AMSU-A radiances, especially with respect to using prescribed bias correction and quality control procedures designed for cloud-cleared radiance assimilation. Thus, before being ingested into analysis, the simulated cloud datasets are required to accurately represent radiative properties of the cloud-affected atmosphere in the TC core area. This is a very important and necessary step in the application of cloudy radiances in a data assimilation system.

4. Case description and experimental design

As an initial attempt to reveal the potential of hybrid data assimilation for the direct assimilation of satellite radiances in the TC core area, this methodology was applied for one major hurricane case, Hurricane Danielle (2010). Danielle spanned the period of 21–30 August 2010 and maintained hurricane strength beginning at 1800 UTC 23 August (Fig. 2a). In response to a new weakening in the subtropical ridge over the central Atlantic, a decrease in shear led to a gradual strengthening of the storm on 26 August. Danielle reached an intensity of 85 kt (1 kt = 0.5144 m s^{-1}) at 1200 UTC 26 August with minimum central pressure of 973 hPa (Fig. 2b). Danielle eventually recurved southeast of Bermuda, never posing a threat to land (Beven and Blake 2013). High-resolution visible satellite images from the *Geostationary Operational Environmental Satellite-13* (*GOES-13*) (Figs. 2a and 2b) show that the clouds in a mature stage of Danielle are dominated by upper-level cirrus and cirrostratus, and there are rough tops of convective clouds penetrating through the smooth cirrostratus. At 1215 UTC 26 August, Danielle is an increasingly well-organized storm (Fig. 2b). The most striking feature around that time are the organized cloud bands spiraling anticyclonically outward, with a visible eye in the central core.

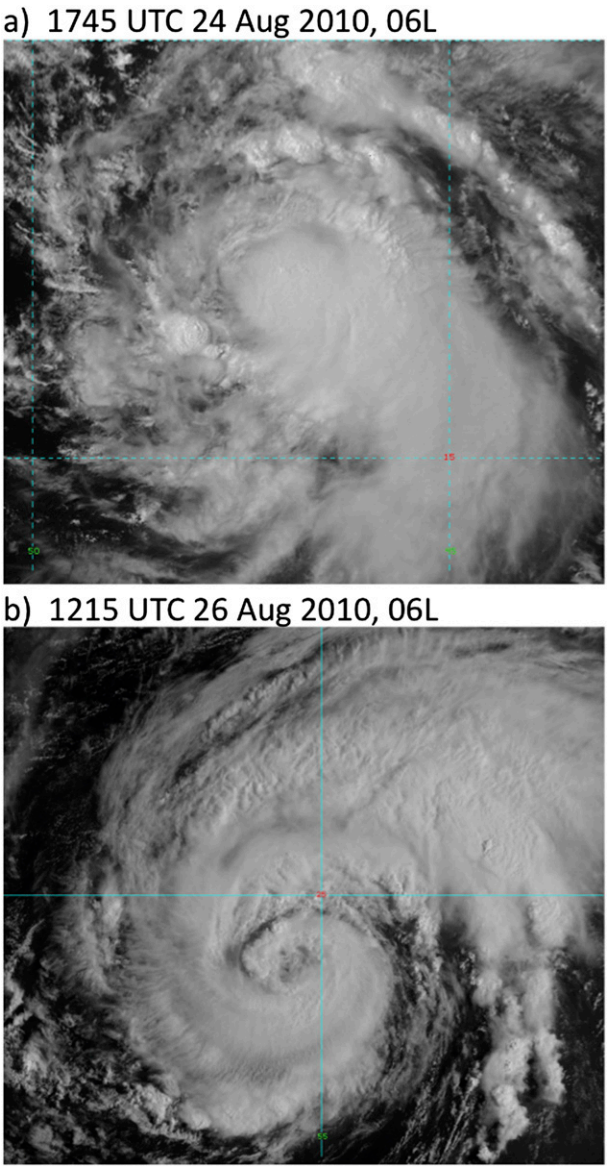

FIG. 2. *GOES-13* visible satellite images at (a) 1745 UTC 24 Aug and (b) 1215 UTC 26 Aug 2010.

Since the aim of this study is to examine the impact of assimilating AMSU-A radiances in the TC core area, no other observations were assimilated. This approach provides an uncomplicated way to examine analysis increments of microphysical and thermodynamic variables induced by AMSU-A radiances. To evaluate the assimilation of cloud-affected AMSU-A radiances in the TC core area, two primary experiments are designed:

TABLE 1. The experimental design for the MLEF-HWRF 6-h cycling data assimilation system from 1200 UTC 24 Aug to 1800 UTC 26 Aug 2010. Different combinations of assimilated observations and forward models are indicated in column 2 and 3, respectively.

Expt	Obs (channel No.)	Forward model
CTL	—	—
ASR	1–8, 15	Cloudy
CSR	1–8, 15	Clear
SND	5–8	Cloudy

(i) the control experiment (CTL), which corresponds to the current operational practice of no data assimilation in TC core, and
(ii) sounding and window channel radiance assimilation (all channel radiances; ASR), which corresponds to a possible extension of the operational practice to assimilate both sounding and window channel radiances in the TC core with the proposed cloudy approach in section 3b.

Two sensitivity experiments were also conducted to evaluate the impact of modeling clouds, by including cloud-guess profiles, and of omitting cloud-relevant channels in observations:

(iii) clear-sky radiance (CSR) assimilation, which is similar to ASR, but uses forward models in cloud-cleared conditions as the operational setting (i.e., no cloud-guess profiles are incorporated in forward models) and
(iv) sounding channels radiance assimilation (SND), which is similar to ASR, but excludes channels with weighting functions peaking below 700 hPa (i.e., channels 1–4 and 15). Since the lower-level peaking channels are more sensitive to cloud liquid water than other temperature sounding channels, the intention of this experiment is to identify if the hybrid data assimilation method, by varying the total-column condensate to fit channels 1–4, and 15, will improve the exclusive use of the temperature sounding channels. Observation errors used in analysis are taken from NCEP statistics.

Table 1 can be referred to for a more detailed description of the experimental design.

Direct assimilation of satellite radiances using hybrid data assimilation with a regional model describing the TC core is fairly new and to the authors' knowledge has not yet been evaluated in any of the peer-reviewed literature. This configuration makes it more difficult to assess the benefits of satellite radiances because the assimilation cycle and model integration time are usually no longer than 3–4 days due to the small domain sizes. It is important to include a sufficient number of cycles so that (i) the accumulated statistics on analysis–forecast performance are meaningful and (ii) representative storm features are sampled. The MLEF-HWRF cycling system provides enough cases and addresses both of these issues. A total of nine cycles for each experiment were conducted, starting at 1200 UTC 24 August 2010, and ending at 1800 UTC 26 August 2010. The assimilation cycle interval is 6 h. The HWRF initial conditions at 1200 UTC 24 August 2010 are interpolated from the global analysis fields from GFS. The analysis is modified by the removal of the GFS vortex and the insertion of a bogus vortex based on theoretical considerations and HWRF climatology. This vortex is relocated and modified so that the initial storm position, structure, and intensity conform to the National Hurricane Center (NHC) storm message provided by the TC vitals. In the 2012 operational HWRF system, the storm is further modified using observations and the GSI system in the storm's environment. In this study, our initialization scheme skips the GSI analysis step in the operational HWRF vortex initialization. Note that the modified HWRF vortex initialization is only used at the start time of MLEF-HWRF cycling runs to restrict the simulated storm. Once the MLEF-HWRF cycling runs begin, the analysis increments are influenced only by AMSU-A radiance assimilation within MLEF.

A 32-member ensemble is used in each experiment; thus, the ensemble size is several orders of magnitude smaller than the size of the control variable. To increase the number of degrees of freedom for the signal (DFS) in the assimilation, we employ error covariance localization (Yang et al. 2009) in the analysis, which includes the interpolation of observation weights in ensemble space. No vertical error covariance localization is applied in this study because of the possible interference with the optimal use of microwave radiances due to the fact that there is not explicit vertical position. Additionally, two minimization iterations of the nonlinear conjugate-gradient algorithm (Zupanski et al. 2008) were used in the data assimilation experiments.

5. Results

In this section, we first compare the simulated TBs with the measured observations under different forward model assumptions. Then, we investigate the structure of the MLEF flow-dependent error estimations and the implications for the cloudy satellite data assimilation. Finally, we show how different configurations can influence the accuracy of TC intensity and structure analyses, as well as short-range forecasts. We verify HWRF (2011) inner-domain forecasts through the 54-h forecasts period against various observations (e.g., NHC best-track data

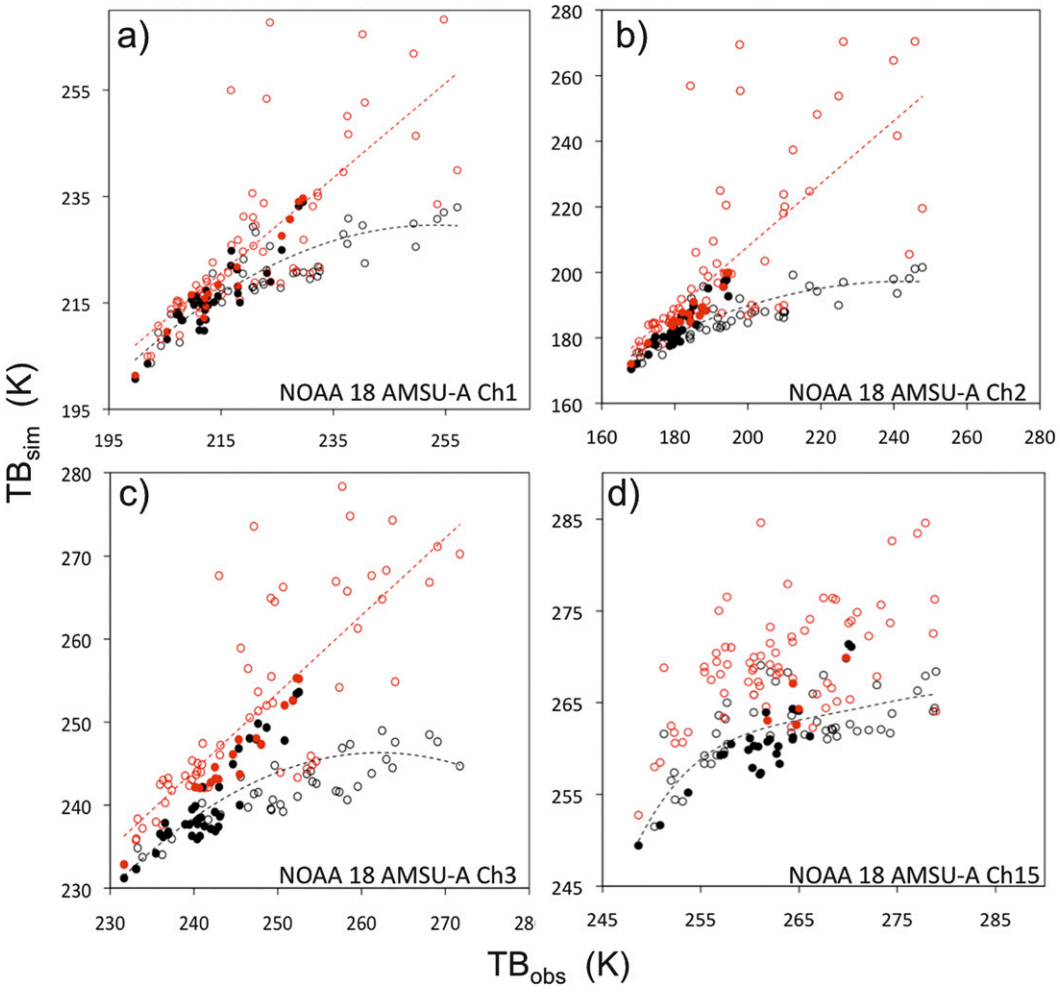

FIG. 3. Comparison of observed TBs with those simulated from the first guess with a cloud ice/water profile calculation (red circles) and without the cloud ice/water profile calculation (black circles) for *NOAA-18* AMSU-A (a) channel 1 (i.e., 23.8 GHz), (b) channel 2 (i.e., 31.4 GHz), (c) channel 3 (i.e., 50.3 GHz), and (d) channel 15 (i.e., 89 GHz), valid at 1800 UTC 24 Aug 2010 in the HWRF inner domain. The total number of observations is 75 following data thinning in a 60 km × 60 km box. Dashed lines denote the trend lines for each scenario. The corresponding red and black dots indicate those data that passed all of the QC procedures and were assimilated into the analysis.

and satellite data), and examine information measures of AMSU-A radiances. Finally, we evaluate the sensitivity of the information content to channel selection and the forward model errors.

a. Validation of the radiance simulations

In Figs. 3 and 4, the observed *NOAA-18* AMSU-A radiances in the HWRF (2011) TC core area are compared to those simulated by the CRTM forward model with and without the inputs of cloud content profiles retrieved from the first guess. Since no bias correction is applied in this step, these comparisons allow for quantifying forward model biases based on different assumptions. Due to the low surface emissivity over the ocean and the sensitivity to the surface temperature (or emissivity), TBs fields simulated from cloud-cleared CRTM at channels 1–3 and 15 (open black dots in Fig. 3) appear to have a cold bias compared to the measured TBs. However, the inclusion of modeled clouds, which have higher emissivities, results in a significant "warming" for warmer atmospheres. Obviously, the overall agreement between the measured and simulated radiances with cloudy radiance simulation is more reasonable for cloudy and rainy conditions. Since channels 4–8 are responsive to average air temperature and atmospheric constituents at increasingly higher altitudes through the troposphere, the simulated TBs are less sensitive to the inclusion of modeling clouds (Fig. 4) compared with those of window channels.

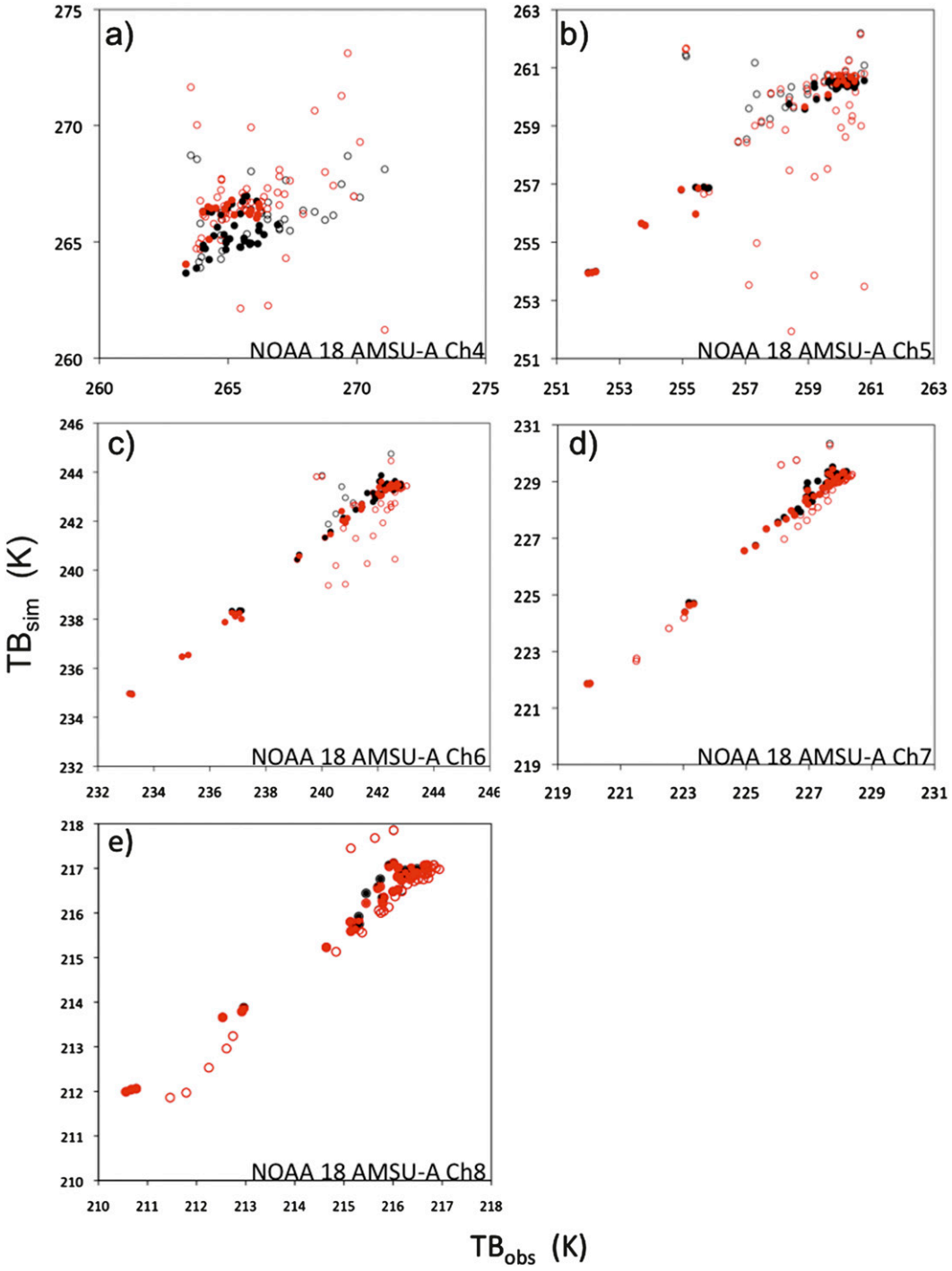

FIG. 4. As in Fig. 3, but for *NOAA-18* AMSU-A (a) channel 4 (i.e., 52.8 GHz), (b) channel 5 (i.e., 53.5 GHz), (c) channel 6 (i.e., 54.4 GHz), (d) channel 7 (i.e., 54.9 GHz), and (e) channel 8 (i.e., 55.5 GHz).

It is also evident that some of the simulated cloudy TBs in channels 5 and 6 have cold biases, although these observations are not ingested into the analysis. The biases are presumably due to the effects of the scattering of large ice/liquid cloud particles that survived from the default quality control procedures.

We further compare the TBs statistics after using cloud-cleared bias correction (BC) and quality control

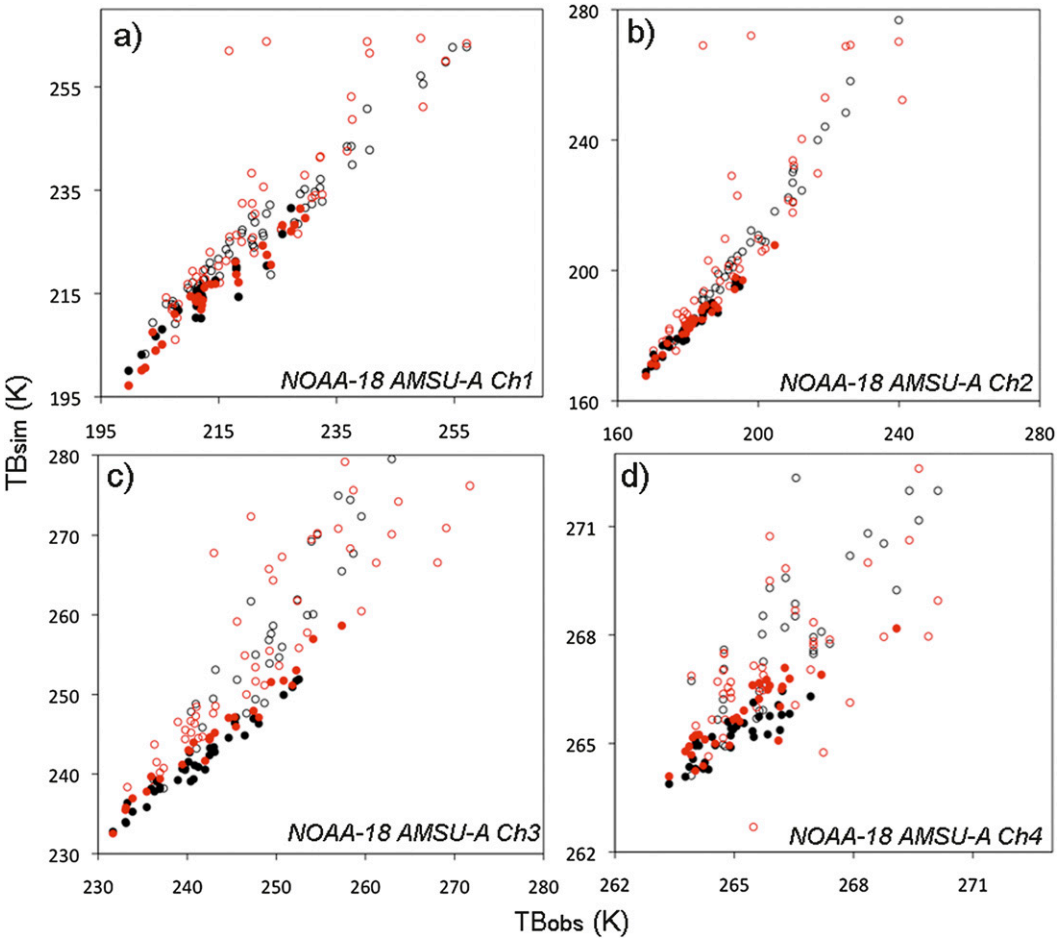

FIG. 5. As in Fig. 3, but for the comparison of observed TBs with the simulated TBs from channels (a) 1, (b) 2, (c) 3, and (d) 4, after being processed using the prescribed bias correction (red circles, ASR; black circles, CSR). The corresponding red and black dots indicate those data that passed all of the QC procedures and were assimilated into the analysis.

(QC) procedures. In Fig. 5, we demonstrate that the prescribed BC scheme has a competitive degree of performance in the cloudy radiance simulation. Furthermore, the resulting distributions after BC and QC are Gaussian, with the maximum number of observations at or near zero, which further confirms that the agreement between the observed and simulated TBs are very good. Simulations without cloud profile inputs generally have low biases, and these errors are only marginally increased in cloudy simulations. Also notice that due to the use of operational QC procedures, the AMSU-A observations are removed if thick clouds or precipitation is detected, which is based on the retrieved cloud liquid water and a retrieved scattering index. Therefore, our assimilation results are valid only for nonprecipitating thin clouds, which are also evident in Fig. 6. In Figs. 6e–h, the areas of significant cloud absorption are highlighted by positive departures, since cloud-cleared radiative transfer simulation for these lower-level peaking channels underestimates the atmospheric contribution added by relatively warm clouds over the radiometrically cold surface. However, a colder temperature departure is evident in Figs. 6a–d. It is worth mentioning that the main differences between the two simulations occur when thick clouds or precipitating conditions prevail, even though only nonscattering/nonprecipitating clouds are assimilated in this study. Nevertheless, it is interesting to examine if the inputs from the model cloud profiles lead to a better simulation of the TC core area structure.

b. Forecast error covariance in hurricane core area

The formulation of the forecast error covariance and the choice of control variables represent two important elements in a multivariate optimization problem. The structure of the forecast error covariance is fundamental since it

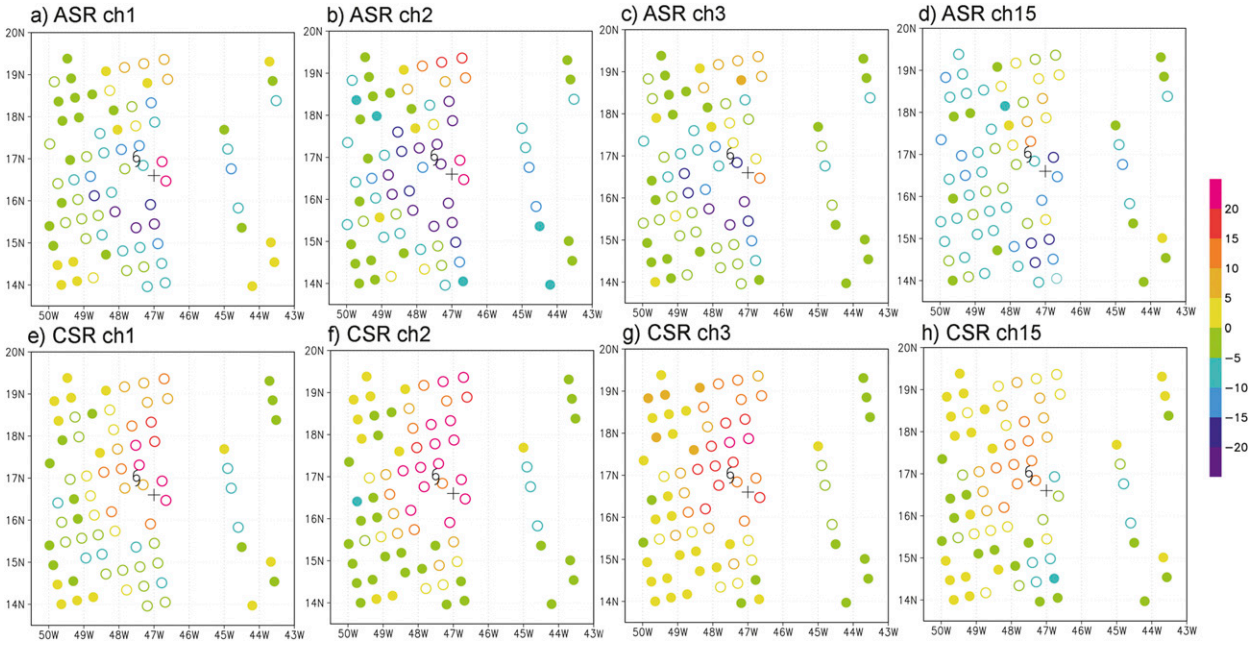

FIG. 6. The *NOAA-18* AMSU-A TBs observations minus the cloudy CRTM-simulated background TBs (K; ASR experiment) before bias correction and data thinning in a 60 km × 60 km box, from channels (a) 1, (b) 2, (c) 3, and (d) 15 at 1800 UTC 24 Aug 2010. Observation locations at which the observed radiances do and do not pass the QC process are indicated by solid dots and open circles, respectively. (e)–(h) As in (a)–(d), but for the CSR experiment. The plus sign denotes the simulated storm, and the observed storm is also indicated. (This is the same for the rest of the figures when applicable.)

defines a mathematical subspace where analysis correction is performed. The square root of the diagonal of this matrix defines a standard deviation that can be used as a measure of uncertainty. It is therefore important to investigate the structure and uncertainty produced by a flow-dependent forecast error covariance in the TC core area.

An example is show in Fig. 7 depicting ensemble errors in Danielle's core region valid at 0600 UTC 25 August 2010. The ensemble error quantifies sample standard deviations for a given variable, and represents the posterior uncertainty provided by the MLEF. It is evident that the forecast uncertainty is significantly larger in the TC core region, not only in hydrometeor mass (i.e., column-integrated CWM), but also in other kinematic and thermodynamic fields. For example, the forecast uncertainty of CWM responds to the high-CWM region. In the vertical cross section, the errors in temperature perturbation (Fig. 8a) are tilted with the radius of maximum wind (RMW), shown in Fig. 8b. The significant forecast uncertainty in low-level wind fields (Fig. 8b), which is related to variations of moist convection in the TC core region, is especially large near the ocean interface and close to the RMW. Larger values indicate the potential for larger corrections from observations in this area during the data assimilation procedure. These results also indicate that the forecast errors evolve with time, propagate with the flow, and can be determined by the underlying storm dynamics.

Through auto- and cross covariance, the information from a single observation can spread to nearby locations and to other variables as well. To illustrate how error covariance responds to an isolated unit perturbation generated by a single observation, we consider a single pseudo-observation of temperature at model level 23 (about 400 hPa) (Fig. 9). This would correspond to an observation of AMSU-A channel 6 radiance sensitive to temperature at location C (20.42°N, 52.88°W). Figures 9a and 9b show the horizontal responses of the temperature and CWM fields, respectively, at the same level. The autocovariance of the temperature indicates a positive response at the observation location, as is expected. The same is true for the CWM response to temperature perturbation (Fig. 9b), indicating that warming implies more clouds. In addition, the horizontal response between the temperature perturbation and wind indicates a divergence, which is also evident as vortex weakening. Figure 9c shows the vertical response of CWM to temperature perturbation. It is evident that there is strong vertical correlation between forecast errors in temperature and hydrometeor content, implying an impact on the analysis throughout the vertical column. In other words, if an AMSU-A channel 6 observation senses warming temperatures at one location, this information will be extended to generate an analysis response in the hydrometeor content in the nearby

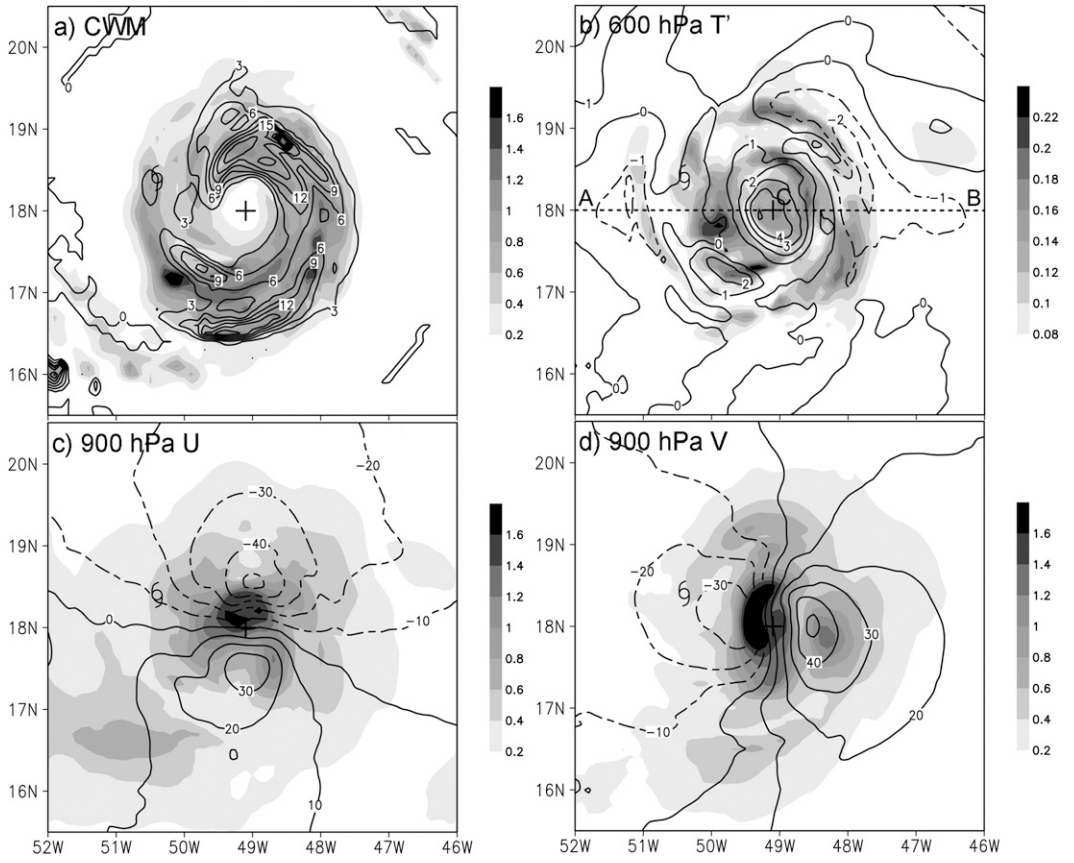

FIG. 7. The horizontal distribution of the optimal analysis state (solid/dashed lines) and the standard deviation (shading) of (a) the vertical cumulated CWM (kg m^{-2}), (b) the temperature perturbation (K) at 600 hPa, (c) u (m s^{-1}) at 900 hPa, (d) v (m s^{-1}) at 900 hPa. All figures are valid for the analysis at cycle 3 (i.e., 0600 UTC 25 Aug 2010).

column and, therefore, influences the cloud analysis throughout the troposphere.

c. *Verification of assimilation results against observations*

Assimilation statistics in Table 2 shows that the observations minus the analysis (OMA) RMS errors over the whole data assimilation period are indeed lower than the observations minus the background (OMB) ones for almost all active channels in the ASR experiment, indicating a positive impact of analysis. Similar results can be found in other radiance assimilation experiments. The forecast tracks of Danielle obtained from the MLEF-HWRF 6-h cycling system are also compared

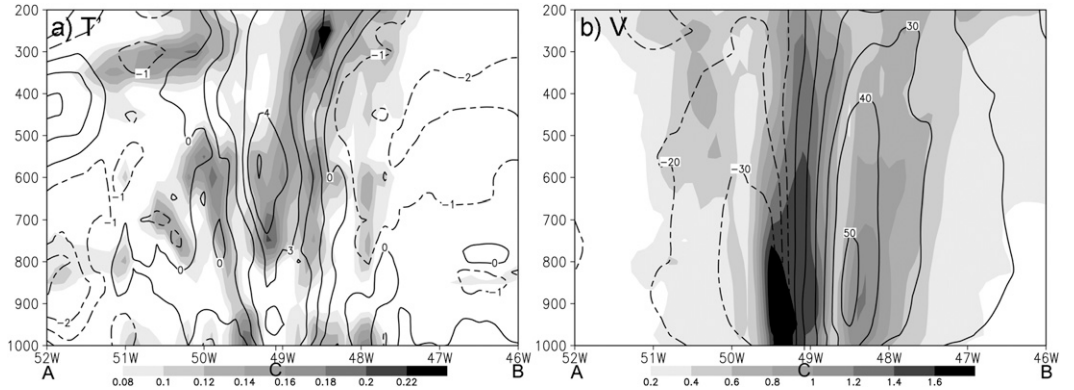

FIG. 8. As in Fig. 7, but for the vertical cross section of (a) T perturbation (K) and (b) v (m s^{-1}), along the latitude of the storm center at 18°N.

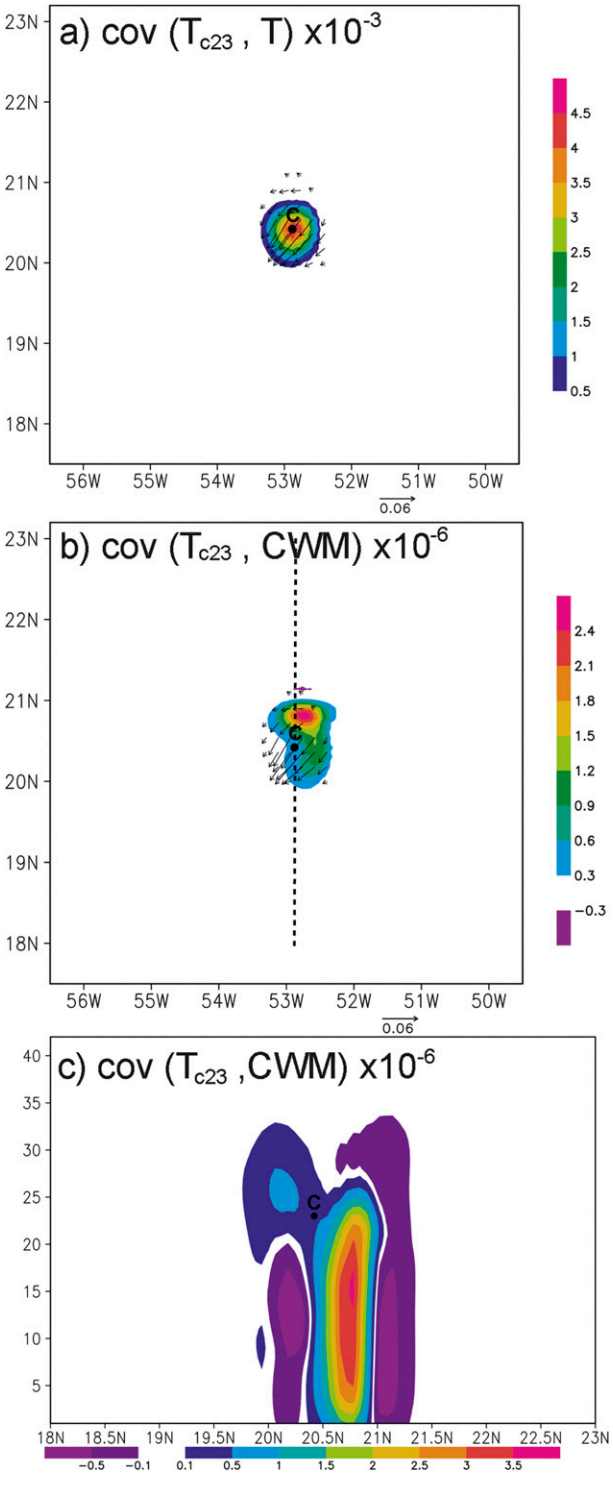

FIG. 9. Background error covariance, illustrated by plotting a portion of the error covariance corresponding to a single observation perturbation on temperature at model level $A = 23$ (about 400 hPa), 20.42°N, 52.88°W, valid at 1800 UTC 25 Aug 2010. (a) Horizontal error autocovariance of T_{c23} and T at $Z = 23$. (b) Horizontal error cross covariance of T_{c23} and CWM at $Z = 23$. (c) Vertical error cross covariance of T_{c23} and CWM at 52.88°W. The horizontal error cross covariance of T_{c23} and wind at $Z = 23$ is also indicated in (a) and (b) by the vectors.

with the NHC best-track data (Fig. 10). The forecast tracks generally agree with the observed track, in which the observed storm turned northwestward later on 25 August.

To further demonstrate the system's capability in reproducing rapid deepening of Danielle, the time series of the minimum mean sea level pressure (MSLP) 6-h forecasts are compared with the NHC best-track data (Fig. 11).[2] Since the 6-h forecast initialized with the analysis obtained by the radiance assimilation at a previous analysis time was used as a background field, the impact of AMSU-A radiance observations propagates gradually into the atmospheric levels, where no observations are available (e.g., the MSLP fields). The HWRF vortex initialization tends to overestimate the MSLP of Danielle at the start time of the data assimilation (i.e., 1200 UTC 24 August 2010) in this study. Although the CTL produced a deeper storm than was observed during the 54-h data assimilation period, the MSLP forecast trend is comparable to the observations. For both the ASR and CSR experiments, during the first 24-h period, the simulated MSLP decreased at a rate slower than the CTL experiment, and more similar to the observed. During the last 30 h, the storms in CSR and SND keep weakening, while the deepening trend of the ASR storm became closer to the observed after cycle 5, and eventually matched the best-track storm MSLP after cycle 8. The difference is apparently due to the unique information extraction capability of the ASR approach.

Now let us shift our attention to the verification of the storm vortex-scale features, using the combined sum of the hydrometeor variables (i.e., CWM). The simulated column-integrated CWM indicates how well the model predicts the precipitation field and the rainfall rate. Figure 10a displays a *MetOp-A* AMSU-A-retrieved precipitation rate map valid at about 1 h later than those in Figs. 12b–e. It is interesting to note that the precipitation pattern in Fig. 10a generally agrees with the visible satellite imagery around this time (Fig. 2b) and the idealized plan-view radar signature of a tropical cycle presented in Hence and Houze (2012, their Fig. 1). In Fig. 12a, the eyewall with about 50-km radius is shown as a semicircular ring of heavy convective precipitation. The rainbands closest to the eyewall, about 200 km from the TC center, are dominated by stratiform precipitation, with broad uniform coverage and very little convective precipitation. In the outer region, organized rainbands spiraled outward in the northern

[2] MSLP is an integral quality and captures aspects of both the magnitude wind and the structure of the wind field and is better suited for intercomparisons of modeled TC structures.

TABLE 2. Data usage statistics related to the ASR experiment. These include the number of observations ingested after data thinning, and passing all QC processes for all channels and cycles, as well as RMS errors of AMSU-A observation departures from the background (OMB) and from the analysis (OMA). If the RMS error of OMA is lower than that of OMB, it is in boldface. Calculations were carried out in the HWRF inner domain over nine cycles from 1800 UTC 24 Aug to 1800 UTC 26 Aug 2010.

	Channel 1	Channel 2	Channel 3	Channel 4	Channel 5	Channel 6	Channel 7	Channel 8	Channel 15
					Cycle 1				
No. of obs	27	26	26	30	47	51	36	12	15
OMB	2.292	2.663	2.113	0.766	0.367	0.277	0.425	0.445	2.839
OMA	**2.078**	**2.451**	**2.112**	**0.633**	**0.343**	0.281	**0.41**	**0.389**	**2.346**
					Cycle 3				
No. of obs	20	20	22	22	41	48	51	10	18
OMB	2.16	2.028	1.442	0.643	0.338	0.24	0.354	0.418	2.538
OMA	**2.103**	**1.63**	**1.388**	**0.641**	**0.287**	**0.204**	**0.349**	**0.406**	**2.267**
					Cycle 5				
No. of obs	24	25	32	33	52	53	82	42	20
OMB	2.35	1.76	2.15	0.488	0.299	0.277	0.324	0.361	2.396
OMA	**2.258**	1.948	2.262	**0.455**	**0.292**	**0.228**	**0.322**	0.366	**2.263**
					Cycle 6				
No. of obs*	17	16	19	19	49	58		15	17
OMB	1.994	2.897	1.780	0.567	0.326	0.183		0.410	2.373
OMA	**1.543**	**2.894**	**1.641**	**0.555**	0.330	0.20		0.418	**2.076**
					Cycle 7				
No. of obs	27	30	32	32	62	65	75	29	27
OMB	2.726	2.099	1.439	0.39	0.282	0.182	0.294	0.341	1.619
OMA	**2.651**	***2***	1.475	**0.369**	**0.278**	**0.171**	**0.289**	**0.329**	1.849
					Cycle 9				
No. of obs	14	14	18	18	34	40	52	32	15
OMB	2.722	2.713	1.686	0.430	0.364	0.228	0.294	0.380	1.945
OMA	**2.615**	**2.400**	1.738	**0.386**	**0.347**	**0.227**	**0.250**	0.424	**1.613**

* AMSU-A observations from *MetOp-A* assimilated in this cycle; otherwise those from *NOAA-18* are assimilated.

quadrant of the storm. All of these features are asymmetric, with primary rainbands located on the downshear side. In Fig. 12c, the ASR-simulated storm size, the cloud condensate distribution, and the area of intense convection compare favorably to the distribution of observed precipitation. In particular, the ASR reproduced organized rainbands that spiraled outward along the north edge of the eyewall with an intense convective center embedded in the rainbands in the northeastern quadrant. The active convection center corresponds to the maximum rainfall core of greater than 20 mm h^{-1} in Fig. 12a. Also well reproduced are weaker centers embedded within the stratiform precipitation on the inner side of the maximum rainfall center. Although the ASR experiment reproduces most of the significant cloud features, a detailed comparison shows a few deficiencies with the simulation. For example, the observed precipitation rate map displays an eyewall with a radius of about 50 km, which is not reproduced in any experiment. Additionally, the ASR experiment also underestimates the radius of the outer rainbands in the northeastern quadrant. These deficiencies are likely related to the relatively coarse horizontal resolution (i.e., 9 km) of the HWRF (2011) inner domain, which cannot resolve intense convective cells at a scale of a few kilometers within the eyewall. It is expected that the 2012 triple-nested HWRF system with 3-km horizontal resolution near the hurricane core can further address these shortcoming (Tallapragada et al. 2012).

By contrast, the CTL-simulated cloud condensate distribution differs markedly from the observations and the ASR experiment. The CTL simulation exhibits two convective centers embedded within the ''distant rainbands'' (Houze 2010) in the northern quadrant. In addition to the significant departures in storm deepening after the first 24 h of integration in the CSR case, compared with the CTL and ASR experiments (Fig. 12), it is also obvious at cycle 7 that similar departures are seen in the CSR cloud and MSLP distributions (Fig. 12d). It is worth noting that the SND experiment, to a certain extent, reproduced the horizontal distribution of the column condensate in the northeast quadrant, such as the intense convective center and the stratiform region on its inner side. However, the deficiency of the SND experiment in surface wind and MSLP intensity indicates that the reproduction to the realistic cloud structure is attributed to assimilating lower-peaking channels of cloudy satellite radiances. Overall, the ASR approach produced a storm that is most similar to the observed

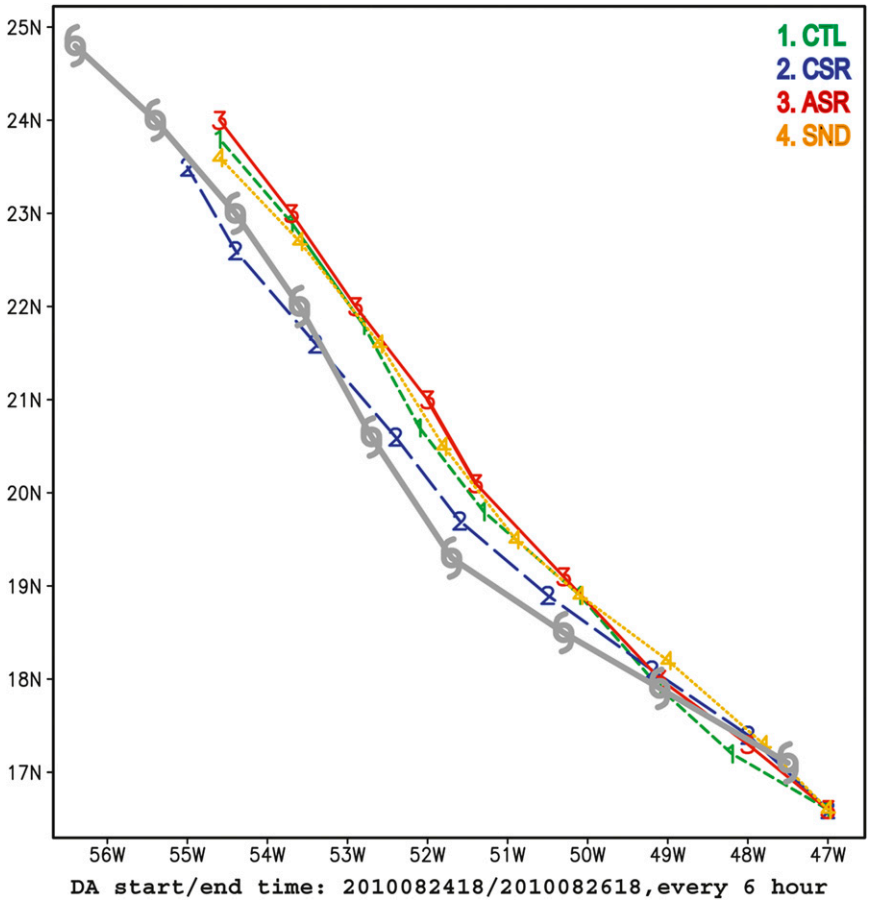

FIG. 10. Tracks of Hurricane Danielle from the 6-h best-track data (denoted by the TC symbol) from the NHC and the CTL/CSR/ASR/SND experiment forecasts are given between 1800 UTC 24 Aug and 1800 UTC 26 Aug 2010 every 6 h.

storm in many aspects, compared to the other experiments. In particular, the simulated asymmetry in the convective structure has important implications with respect to the improvement of quantitative precipitation forecasts (QPFs), wave height forecasts, and severe wind warnings if the storm is about to make landfall.

Information content in ensemble subspace (Zupanski et al. 2007) was developed using information theoretical concepts elucidated by Shannon and Weaver (1949) and through the application of their technique to atmospheric science by Rodgers (2000). In MLEF, the amount of information contained in the observations is quantified by comparing the effective signal to noise ratios. This is accomplished practically through the analysis of the information matrix in the ensemble subspace, of dimensions $N_{\text{ens}} \times N_{\text{ens}}$, which holds the key the understanding and quantifying the differences between various forward models and the observational data. This study uses the same definition and formula as Zupanski et al. (2007). The overall features of the information content analysis (i.e., the spatial distribution of DFS) have been gathered together in Fig. 13, which shows the information content that is added through the combination of different forward models and channel selection (i.e., ASR/CSR/SND experiments; see Table 1). In Fig. 13, we plotted the DFS obtained in experiments with 10×10 subdomains (e.g., pixels). The DFSs are calculated for each of the 100 local blocks and quantify the impact of the observations in each local block. The flow-dependent DFS indicates the utility of AMSU-A radiances in the HWRF (2011) inner domain. In the first cycles, the correlated forecast differences imply a reduction of DFS in the information content or the forecast error covariance due to the utility of the time-shifted ensemble perturbations at the beginning of the data assimilation. However, the number of DFSs quickly increases given that there is sufficient error growth in ensemble prediction with HWRF. This increase is particularly evident near the center of the TC core area for the ASR experiment and to a lesser extent

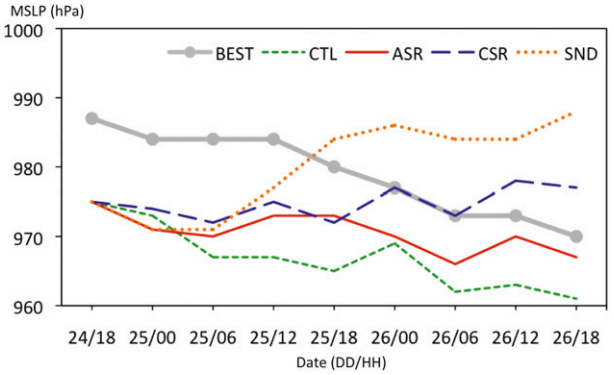

FIG. 11. Time series of the MSLP (hPa) and NHC best-track data (thick gray line), and MLEF-HWRF 6-h forecasts between 1800 UTC 24 Aug and 1800 UTC 26 Aug 2010 every 6 h (i.e., cycles 1–9).

for the SND experiment, suggesting that the observations are influencing the region of the TC that is often poorly observed in the current HWRF due to the clear-sky assumption. It is also indicated that the ASR configuration provides the most integrated information over all of the cases shown. These results further demonstrated that an entropy-based definition of information content provides a powerful metric for evaluating the utility of a set of observations and simulated satellite radiances in a hybrid data assimilation method.

6. Conclusions and discussion

Currently, no inner-core satellite radiances are directly assimilated in NCEP operational NWP models, including both GFS and HWRF systems. However, these observations of clouds and precipitation may hold the key to improving vortex initialization and ultimately TC intensity prediction. In this study, a prototype hybrid variational–ensemble data assimilation system (HVEDAS) is used to identify the impact of the direct assimilation of satellite radiances in the TC core area. The assimilation experiments are conducted using MLEF with NOAA operational codes that include the atmospheric component of the HWRF (2011) model and the forward components of the GSI analysis system and the CRTM. Specifically, the AMSU-A radiances from *NOAA-18* and *MetOp-A* are assimilated into Hurricane Danielle (2010) with the maximum likelihood ensemble filter (MLEF), which better addresses the nonlinearity of the observation operators than more common EnKF methodologies by employing an iterative minimization of a cost function. The new approach has additional components required for allowing cloud-affected radiance assimilation, such as augmenting the analysis control variables to include clouds and adding cloud-guess profiles in the forward models. The CRTM forward model biases are first calculated in the HWRF

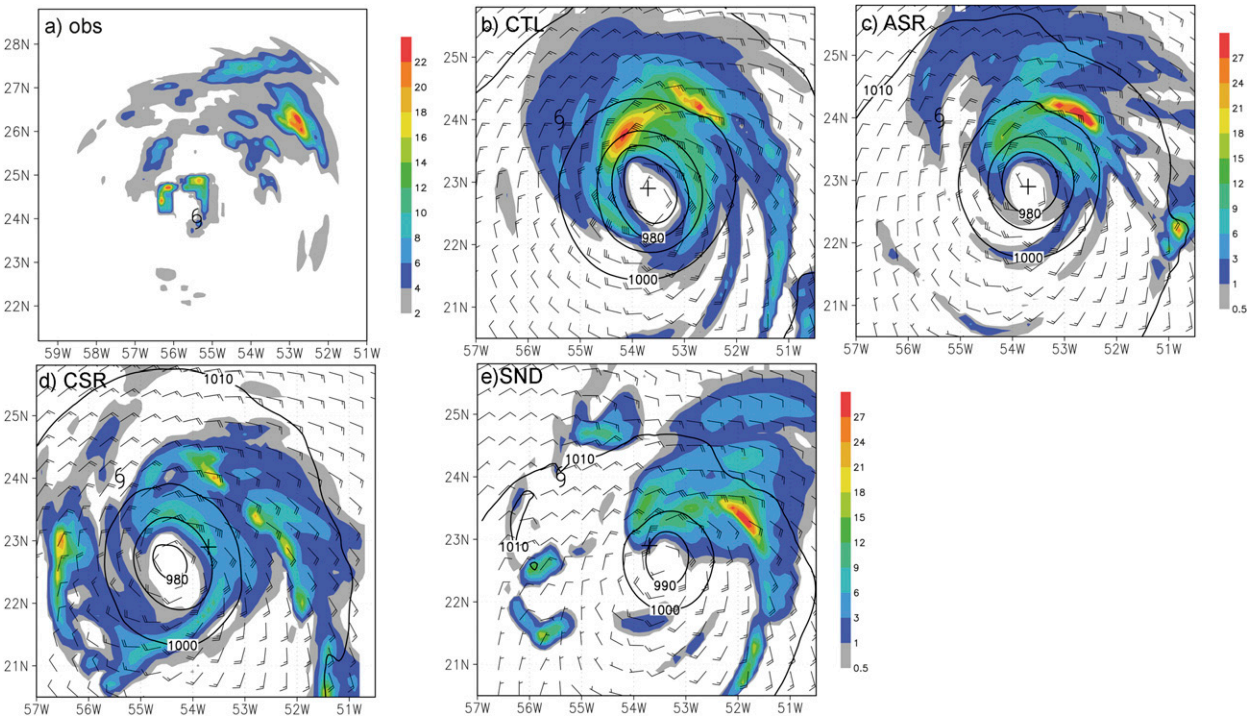

FIG. 12. (a) AMSU-retrieved precipitation rate map from *MetOp-A* at 1311 UTC 26 Aug 2010 (mm h^{-1}). Distribution of the 6-h CWM (colored; Kg m^{-2}) forecasts start from cycle 7 analyses of the (b) CTL, (c) ASR, (d) CSR, and (e) SND experiments, superposed with MSLP and 10-m above wind barbs, valid at 1200 UTC 26 Aug 2010.

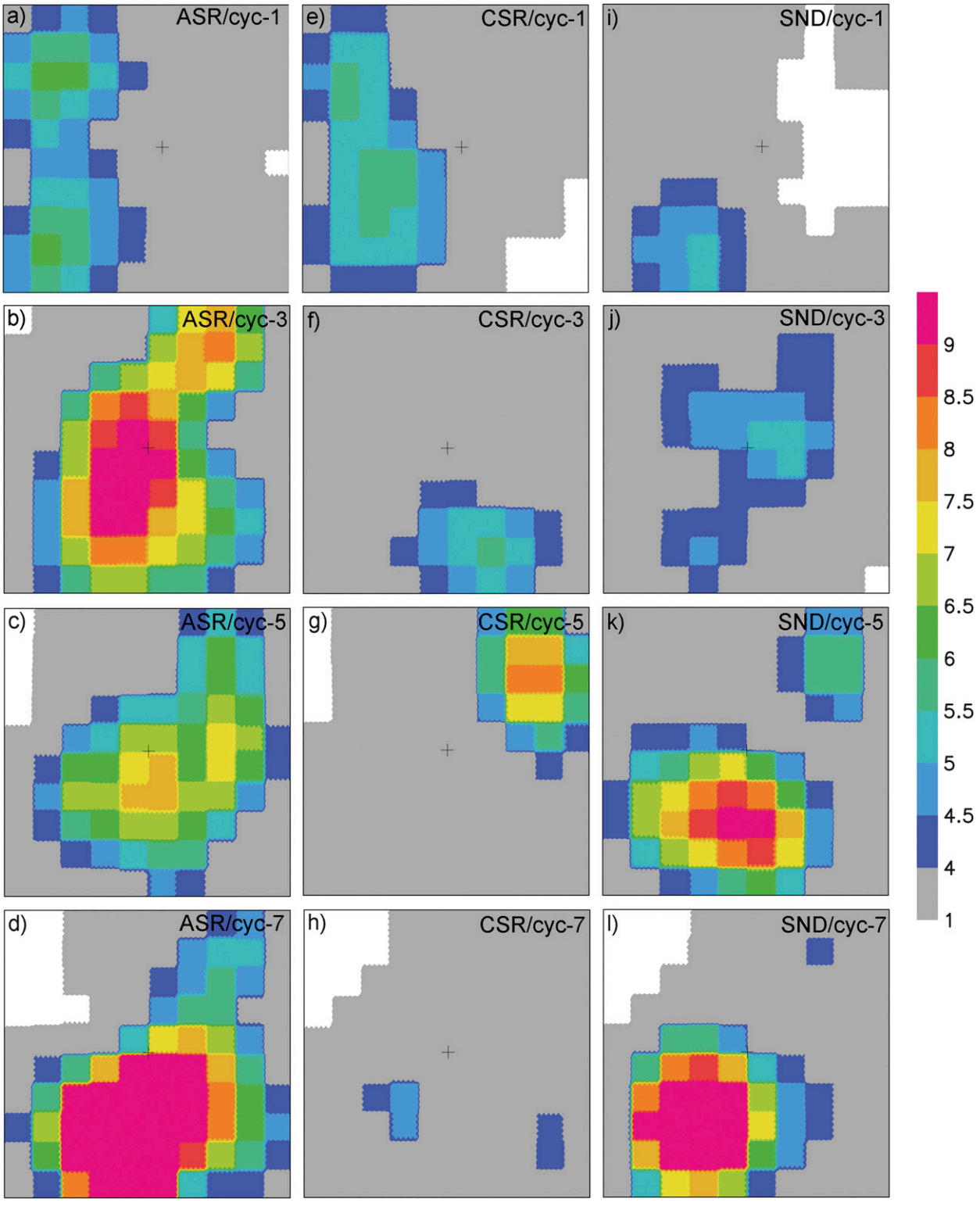

FIG. 13. Information content results of the assimilated observations (DFSs) calculated in the distinct data assimilation configurations are shown for cycles 1, 3, 5, and 7. The DFS are nondimensional quantities. All figures are plotted in an HWRF inner domain (i.e., with a scale of $6° \times 6°$) centered at the simulated storm center. Larger values indicate a greater influence of the observation in the data assimilation.

inner domain based on both cloud-cleared and cloudy radiance simulation assumptions, which are required for the assimilation of cloudy satellite radiances. The results suggest that the cloudy AMSU-A radiance simulation outperforms the cloud-cleared simulation across all *NOAA-18* AMSU-A channels and that the operational data processing procedures are correctly adjusting for any remaining systematic differences on a TC core area basis. It is also shown that through the prescribed ''cloud cleared'' bias correction and quality control procedures, the simulated and observed TB fields show good agreement for all *NOAA-18* AMSU-A channels.

The ensemble uncertainty analysis is found to be highly anisotropic and time dependent. The horizontal autocorrelation of a pseudo-AMSU-A channel 6 observation produces an isotopic, Gaussian-like shape as a function of distance. In turn, complex microphysical processes in the TC core area imply that hydrometeor mass variables will be cross correlated with temperature and produce different horizontal and vertical structure functions. The flow-dependent structures of error cross covariance between temperature and hydrometeor variables provide a means for observation information on temperature affected by nonscattering clouds to influence hydrometeor fields as well (e.g., Fig. 9). Furthermore, our results demonstrate the necessity of gaining a better understanding of the error growth mechanism and the related storm dynamics for the TC core region.

The performance of the HVEDAS and the value of cloudy radiance assimilation added to the analyses and forecasts of Danielle (2010) core area are assessed by a comparison with observations. In particular, we performed cycling data assimilation experiments at 6-h intervals for a length of 54 h to examine the performance when reproducing the observed storm track (Fig. 10), intensity/MSLP (Fig. 11), and vortex-scale structure (Fig. 12). In general, the impact on the storm track was marginal. However, a particularly encouraging result was the improvement in the storm intensity forecasts over the operational control experiment. The proposed ASR approach tends to outperform the operational and cloud-cleared radiance experiments. With the cloud-affected AMSU-A radiance assimilated, the system reasonably captures the rapid deepening stage of Hurricane Danielle, and reproduces a measurable positive impact on the TC intensity prediction, as well as on the hydrometeor structures through multivariate correlations of microwave radiances and thermodynamical fields, and model integration. The results also show that the entropy-based information content of the data, as measured by the degrees of freedom for signal (DFS), was significantly increased, implying a more efficient use of the observations in the ASR experiment (Fig. 13).

Although a case study, this study provides insights and potential solutions for future TC prediction, especially for the TC structure including intensity forecasts. Our results suggest that a hybrid data assimilation algorithm could provide an objective, observation-based way of incorporating a dynamically consistent vortex with reasonable asymmetries into the initial conditions of the current triple-nested 2012 operational HWRF system operating at 3-km horizontal resolution near the hurricane core. This study paves the way for the assimilation of other data types in the cores of TCs. Data from new microwave sounders and scatterometers, as well as aircraft-based data, if used within this framework, offer even further opportunities to improve the TC vortex initialization of operational forecast models.

Acknowledgments. We wish to thank three anonymous reviewers for their constructive comments. This work was supported by the NOAA Hurricane Forecast Improvement Project (HFIP) and the Joint Center for Satellite Data Assimilation program through Grant NA10NES4400012. This work was also partially supported by the National Science Foundation Collaboration in Mathematical Geosciences Grant ATM-0930265. The computing for this study was performed at NOAA/NCEP computing facilities, and Supercomputer for Satellite Simulations and Data Assimilation Studies (S4) system and services provided by SSEC and STAR. The views, opinion, and findings contained in this article are those of the authors and should not be construed as an official NOAA or U.S. government position, policy, or decision.

REFERENCES

Barker, D. M., W. Huang, Y. R. Guo, and Q. N. Xiao, 2004: A three-dimensional data assimilation system for use with MM5: Implementation and initial results. *Mon. Wea. Rev.,* **132,** 897–914.

Bauer, P., A. J. Geer, P. Lopez, and D. Salmond, 2010: Direct 4D-Var assimilation of all-sky radiances. Part I: Implementation. *Quart. J. Roy. Meteor. Soc.,* **136,** 1868–1885.

Baum, B. A., P. Yang, A. J. Heymsfield, S. Platnich, M. D. King, Y.-X. Hu, and S. T. Bedka, 2005: Bulk scattering models for the remote sensing of ice clouds. Part II: Narrowband models. *J. Appl. Meteor.,* **44,** 1896–1911.

Bernardet, L., and Coauthors, 2012: Hurricane WRF: 2012 Operational implementation and community support. *Proc. 13th WRF Users' Workshop,* Boulder, CO, NCAR, 2.2. [Available online at http://www.mmm.ucar.edu/wrf/users/workshops/WS2012/abstracts/2.2.htm.]

Beven, J. L., II, and E. S. Blake, 2013: Atlantic hurricane season of 2010. *Mon. Wea. Rev.,* in press.

Dee, D. P., and S. Uppala, 2009: Variational bias correction of satellite radiance data in the ERA-Interim reanalysis. *Quart. J. Roy. Meteor. Soc.,* **135,** 1830–1841.

DeMaria, M., 2009: A simplified dynamical system for tropical cyclone intensity prediction. *Mon. Wea. Rev.,* **137,** 68–82.

Derber, J. C., and W.-S. Wu, 1998: The use of TOVS cloud-cleared radiances in the NCEP SSI analysis system. *Mon. Wea. Rev.,* **126,** 2287–2299.

Ferrier, B. S., 2005: An efficient mixed-phase cloud and precipitation scheme for use in operational NWP models. *Eos, Trans. Amer. Geophys. Union,* **86** (Spring Meeting Suppl.), Abstract A42A-02.

Gall, R., J. Tuttle, and P. Hildebrand, 1998: Small-scale spiral bands observed in Hurricanes Andrew, Hugo, and Erin. *Mon. Wea. Rev.,* **126,** 1749–1766.

Gopalakrishnan, S., and Coauthors, 2011: Hurricane Weather Research and Forecasting (HWRF) model scientific documentation. Development Tech Center Tech. Rep., 75 pp.

Harris, B. A., and G. Kelly, 2001: A satellite radiance-bias correction scheme for data assimilation. *Quart. J. Roy. Meteor. Soc.,* **127,** 1453–1468.

Hence, D. A., and R. A. Houze Jr., 2012: Vertical structure of tropical cyclone rainbands as seen by the TRMM Precipitation Radar. *J. Atmos. Sci.,* **69,** 2644–2661.

Hou, Y.-T., S. Moorthi, and K. A. Campana, 2002: Parameterization of solar radiation transfer in the NCEP models. NCEP Office Note 441, 34 pp. [Available online at http://www.emc.ncep.noaa.gov/officenotes/newernotes/on441.pdf.]

Houze, R. A., Jr., 2010: Clouds in tropical cyclones. *Mon. Wea. Rev.,* **138,** 293–344.

Janjić, Z. I., 2003: A nonhydrostatic model based on a new approach. *Meteor. Atmos. Phys.,* **82,** 271–285.

——, J. P. Gerrity Jr., and S. Nickovic, 2001: An alternative approach to nonhydrostatic modeling. *Mon. Wea. Rev.,* **129,** 1164–1178.

Kidder, S. Q., M. D. Goldberg, R. M. Zehr, M. DeMaria, J. F. W. Purdom, C. S. Velden, N. C. Grody, and S. J. Kusselson, 2000: Satellite analysis of tropical cyclones using the Advanced Microwave Sounding Unit (AMSU). *Bull. Amer. Meteor. Soc.,* **91,** 1241–1259.

Kleist, D. T., D. F. Parrish, J. C. Derber, R. Treadon, W.-S. Wu, and S. Lord, 2009: Introduction of the GSI into the NCEP Global Data Assimilation System. *Wea. Forecasting,* **24,** 1691–1705.

Knaff, J. A., M. D. Goldberg, S. Q. Kidder, and R. M. Zehr, 2000: An example of temperature structure differences in two cyclone systems derived from the Advanced Microwave Sounder Unit. *Wea. Forecasting,* **15,** 476–483.

Kurihara, Y., M. A. Bender, and R. J. Ross, 1993: An initialization scheme of hurricane models by vortex specification. *Mon. Wea. Rev.,* **121,** 2030–2045.

Macke, A., J. Mueller, and E. Raschke, 1996: Single scattering properties of atmospheric ice crystals. *J. Atmos. Sci.,* **53,** 2813–2825.

McNally, A. P., 2009: The direct assimilation of cloud-affected satellite infrared radiances in the ECMWF 4D-Var. *Quart. J. Roy. Meteor. Soc.,* **135,** 1214–1229.

Mishchenko, M. I., J. W. Hovenier, and L. D. Travis, (2000): *Light Scattering by Nonspherical Particals: Theory, Measurements, and Applications.* Academic Press, 690 pp.

Pu, Z.-X., X. Li, and J. Sun, 2009: Impact of airborne Doppler radar data assimilation on the numerical simulation of intensity changes of Hurricane Dennis near a landfall. *J. Atmos. Sci.,* **66,** 3351–3365.

Robel, J., cited 2009: NOAA KLM user's guide. NOAA/National Climatic Data Center. [Available online at http://www.ncdc.noaa.gov/oa/pod-guide/ncdc/docs/intro.htm.]

Rodgers, C. D., 2000: *Inverse Methods for Atmospheric Sounding: Theory and Practice.* World Scientific, 238 pp.

Rogers, R., 2010: Convective-scale structure and evolution during a high-resolution simulation of tropical cyclone rapid intensification. *J. Atmos. Sci.,* **67,** 44–70.

——, and Coauthors, 2006: The Intensity Forecasting Experiment: A NOAA multiyear field program for improving tropical cyclone intensity forecasts. *Bull. Amer. Meteor. Soc.,* **87,** 1523–1537.

Shannon, C. E., and W. Weaver, 1949: *The Mathematical Theory of Communication.* University of Illinois Press, 144 pp.

Simmer, C., 1994: *Satellitenfernerkundung Hydrologischer Parameter der Atmosphare mit Mikrowellen*. Verlag, 313 pp.

Skamarock, W. C., J. B. Klemp, J. Dudhia, D. O. Gill, D. M. Barker, W. Wang, and J. G. Powers, 2005: A description of the Advanced Research WRF version 2. NCAR Tech. Note NCAR/TN-468+STR, 88 pp.

Tallapragada, V., and Coauthors, 2012: Operational implementation of high-resolution triple-nested HWRF at NCEP/EMC-A major step towards addressing intensity forecast problem. Preprints, *30th Conf. on Hurricanes and Tropical Meteorology,* Ponte Vedra Beach, FL, Amer. Meteor. Soc. [Available online at https://ams.confex.com/ams/30Hurricane/webprogram/Paper205287.html.]

Wakimoto, R. M., and P. G. Black, 1994: Damage survey of Hurricane Andrew and its relationship to the eyewall. *Bull. Amer. Meteor. Soc.,* **75,** 189–200.

Weng, F., 2007: Advances in radiative transfer modeling in support of satellite data assimilation. *J. Atmos. Sci.,* **64,** 3799–3807.

——, and Q. Liu, 2003: Satellite data assimilation in numerical weather prediction models. Part I: Forward radiative transfer and Jacobian modeling in cloudy atmospheres. *J. Atmos. Sci.,* **60,** 2633–2646.

Wu, W., R. J. Purser, and D. F. Parrish, 2002: Three-dimensional variational analysis with spatially inhomogeneous covariances. *Mon. Wea. Rev.,* **130,** 2905–2916.

Xiao, Q., X. Zhang, C. Davis, J. Tuttle, G. Holland, P. Holland, and P. J. Ftzpatrick, 2009: Experiments of Hurricane initialization with Airborne Doppler radar data for the Advanced Research Hurricane WRF (AHW) model. *Mon. Wea. Rev.,* **137,** 2758–2777.

Yang, S.-C., E. Kalnay, B. Hunt, and N. E. Bowler, 2009: Weight interpolation for efficient data assimilation with the local ensemble transform Kalman filter. *Quart. J. Roy. Meteor. Soc.,* **135,** 251–262.

Yau, M. K., Y. Liu, D.-L. Zhang, and Y. Chen, 2004: A multiscale numerical study of Hurricane Andrew (1992). Part VI: Small-scale inner-core structures and wind streaks. *Mon. Wea. Rev.,* **132,** 1410–1433.

Zhang, F., Y. Weng, J. A. Sippel, Z. Meng, and C. H. Bishop, 2009: Cloud-resolving hurricane initialization and prediction through assimilation of Doppler radar observations with an ensemble Kalman filter. *Mon. Wea. Rev.,* **137,** 2105–2125.

——, ——, J. F. Gamache, and F. D. Marks, 2011: Performance of convection-permitting hurricane initialization and prediction during 2008–2010 with ensemble data assimilation of inner-core airborne doppler radar observations. *Geophys. Res. Lett.,* **38,** L15810, doi:10.1029/2011GL048469.

Zupanski, D., A. Y. Hou, S. Q. Zhang, M. Zupanski, C. D. Kummerow, and S. H. Cheung, 2007: Application of information theory in ensemble data assimilation. *Quart. J. Roy. Meteor. Soc.,* **133,** 1533–1545.

Zupanski, M., 2005: Maximum likelihood ensemble filter: Theoretical aspects. *Mon. Wea. Rev.,* **133,** 1710–1726.

——, I. M. Navon, and D. Zupanski, 2008: The maximum likelihood ensemble filter as a non-differentiable minimization algorithm. *Quart. J. Roy. Meteor. Soc.,* **134,** 1039–1050.